Planck data reconsidered

David N. Spergel, Raphael Flauger, and Renée Hložek

Planck Data Reconsidered

David N. Spergel[1], Raphael Flauger[2,3] & Renée Hložek[1]

[1]*Department of Astrophysical Sciences, Princeton University, Princeton, NJ 08544, USA*
[2]*Institute for Advanced Study, Einstein Drive, Princeton, NJ 08540, USA*
[3]*CCPP, New York University, New York, NY 10003, USA*

The tension between the best fit parameters derived by the Planck team and a number of other astronomical measurements suggests either systematics in the astronomical measurements, systematics in the Planck data, the need for new physics, or a combination thereof. We re-analyze the Planck data and find that the $217\,\mathrm{GHz} \times 217\,\mathrm{GHz}$ detector set spectrum used in the Planck analysis is responsible for some of this tension. We use a map-based foreground cleaning procedure, relying on a combination of 353 GHz and 545 GHz maps to reduce residual foregrounds in the intermediate frequency maps used for cosmological inference. For our baseline data analysis, which uses 47% of the sky and makes use of both 353 and 545 GHz data for foreground cleaning, we find the ΛCDM cosmological parameters $\Omega_c h^2 = 0.1170 \pm 0.0025$, $n_s = 0.9686 \pm 0.0069$, $H_0 = 68.0 \pm 1.1\,\mathrm{km\,s^{-1}Mpc^{-1}}$, $\Omega_b h^2 = 0.02197 \pm 0.00026$, $\ln 10^{10} A_s = 3.082 \pm 0.025$, and $\tau = 0.090 \pm 0.013$. While in broad agreement with the results reported by the Planck team, these revised parameters imply a universe with a lower matter density of $\Omega_m = 0.302 \pm 0.015$, and parameter values generally more consistent with pre-Planck CMB analyses and astronomical observations. We compare our cleaning procedure with the foreground modeling used by the Planck team and find good agreement. The difference in parameters between our analysis and that of the Planck team is mostly due to our use of cross-spectra from the publicly available survey maps instead of their use of the detector set cross-spectra which include pixels only observed in one of the surveys. We show evidence suggesting residual systematics in the detector set spectra used in the Planck likelihood code, which is substantially reduced for our spectra. Using our cleaned survey cross-spectra, we recompute the limit on neutrino species and find $N_{\mathrm{eff}} = 3.34 \pm 0.35$. We also recompute limits on the $n_s - r$ plane, and neutrino mass constraints.

I. INTRODUCTION

Observations of the cosmic microwave background are our most powerful probe of the physical conditions in the early universe and can provide precise and accurate determinations of cosmological parameters. Over the past decade, analyses of the data from the Wilkinson Microwave Anisotropy Probe [1–5] have established a now standard six parameter ΛCDM model for cosmology. In combination with ever-improving ground-based cosmic microwave background data, the most recent being the Atacama Cosmology Telescope (ACT) [6] and the South Pole Telescope (SPT) [7], these measurements have yielded increasingly accurate determinations of cosmic parameters.

The eagerly anticipated Planck satellite was the next major step forward in the study of the cosmic microwave background [8]. The data are of exceptional quality, with excellent noise properties and above-expected performance of the satellite and its components. The data at 30, 44, 70, 100, 143, 217, 353, 545 and 857 GHz provide maps which are not only useful for cosmology, but, through their increased angular resolution, have also improved our understanding of the emission from astrophysical sources in the universe.

One of the most surprising results from the Planck satellite is the measurement of cosmological parameters based on its three central frequencies, 100 GHz, 143 GHz and 217 GHz [9, 10] that finds a higher matter density, $\Omega_m = 0.315^{+0.016}_{-0.018}$, a higher amplitude of matter fluctuations, $\sigma_8 (\Omega_m/0.27)^{0.3} = 0.87 \pm 0.02$, and a lower Hubble constant, $H_0 = 67.3 \pm 1.2\,\mathrm{km\,s^{-1}Mpc^{-1}}$ than previous analyses of CMB data [11]. These new Planck values are all around 2-3 σ discrepant with various astronomical measurements including measurements of the Hubble constant using distance ladders [12, 13], measurements of the matter density using supernova [14] and measurements of the amplitude of matter fluctuations using a variety of techniques: gravitational lensing [15, 16], two and three-point statistics of the SZ map [17–19] and cluster counts with mass determinations based on either SZ measurements [20, 21], X-ray measurements [22, 23], or optical clustering and lensing [24]. These deviations suggest either systematics in the astronomical probes, a failure of the "simple" six parameter ΛCDM model, or systematics in the analysis of the Planck data.

The conclusions of the Planck paper rest at least in part on their analysis of the 217 GHz maps. This is highlighted by the sensitivity of the best-fit n_s to the inclusion of the 217×217 power spectrum shown in Appendix C of Paper XVI [10]. At first sight, the observed shift could be due to the additional data provided by the 217×217 power spectrum. After all, the 217 GHz channel has the highest resolution among the channels used for the Planck analysis. However, the power spectrum made from the 217 GHz data shows a strong departure from the standard model at

$\ell \simeq 1800$ which is not seen at other frequencies, and is thus not of cosmological origin. In addition, the 217 GHz spectra fail a number of null tests shown by the Planck team in Figures 29 and 30 of Paper VI [25]. This suggests that the dependence on the 217×217 data may in part be due to systematics. In Section II, we show that there is not only a significant difference between the Planck 217×217 spectrum and the 100×100, 143×143, and 143×217 spectra around $\ell \simeq 1800$ but also for $\ell \gtrsim 2000$, and that the removal of the 217×217 spectrum from the Planck likelihood analysis alters best-fit parameters by more than expected from simulations.[1]

In Section III, we make use of the higher frequency Planck data at 353 GHz and 545 GHz to recompute the CMB power spectrum and perform an analysis that is much less sensitive to the foreground model. At small angular scales, dusty galaxies are a significant foreground and contribute more to the variance of these maps than the cosmic microwave background fluctuations. Planck's sensitive high-frequency channels trace the sub-millimeter fluctuations in the dusty galaxy distribution well. By minimizing the variance in linear combinations of the lower frequency maps (100, 143 and 217 GHz) with a combination of the 353 or 545 GHz maps: we "clean" the maps. We also use the multi-frequency data to define masks that are both unbiased (relative to the CMB) and use a larger fraction of the sky than the masks used by the Planck team. If we restrict ourselves to the same masks as used by the Planck team, the analysis based on our cleaned spectra agrees well with our analysis of uncleaned survey cross-spectra with the same foreground model as used by the Planck team. However, our cleaning procedure allows us to use significantly more of the sky without biasing the spectra or parameters.

In Section IV, we use the new maps to recompute cosmological parameters. For the ΛCDM model, the parameters systematically shift towards the results of earlier analyses based on WMAP, ACT and SPT [11], decreasing the tension with other astronomical measurements. In this section, we also consider the implications of the new parameters for neutrino properties and for inflationary models.

In Section V, we discuss what might be the origin of the shifts. We show that our cosmological parameters are neither sensitive to the sky fraction used nor to whether we compute the power spectrum from the cleaned maps or instead implement a power spectrum-based correction as is done in the Planck team analysis. We compare our cross-spectra to the detector set spectra used in the Planck analysis. The difference seems to be primarily due to an offset between the released Planck spectra (which we will refer to as 'CAMspec' spectra) and the cross-spectra, suggesting that difference spectra computed between the Planck detector set maps and the survey maps will fail null tests. Some of the shifts when removing the 217×217 data remain even when using the survey cross-spectra. However, the shifts are smaller if the data are cleaned using our procedure and consistent with expectations based on simulations.

II. THE 217× 217 POWER SPECTRUM: A FLY IN THE OINTMENT?

The 217×217 detector set spectra are responsible for a significant amount of the shift in cosmological parameters reported by Planck. To illustrate this, we have used the publicly released Planck likelihood code to run Monte-Carlo Markov Chains for the Planck data (Planck+WP) as used by the Planck team and without the 217×217 data. Table I compares the results of these analyses to the parameters derived from an analysis based on WMAP9 and ACT data [11]. Without the 217×217 data, the Planck results have 20-36% smaller errors than the WMAP9+ACT

TABLE I: Planck versus pre-Planck ΛCDM Cosmological Parameters

	Planck Analysis	No 217×217	WMAP9+ACT
$10\ \Omega_c h^2$	1.199 ± 0.026	1.181 ± 0.027	1.146 ± 0.043
n_s	0.9603 ± 0.0073	0.9661 ± 0.0077	0.973 ± 0.011
H_0	67.3 ± 1.2	68.1 ± 1.2	69.7 ± 2.0
$100\ \Omega_b h^2$	2.205 ± 0.028	2.226 ± 0.029	2.260 ± 0.041
Ω_m	0.315 ± 0.016	0.305 ± 0.016	0.284 ± 0.024

numbers, and the values for $\Omega_c h^2$, H_0 and n_s agree within $1\,\sigma$. The inclusion of the 217×217 power spectrum further

---

[1] From the revised *Planck* publication [10] we know that the difference around $\ell \simeq 1800$ arises from the incomplete removal of the 4K cooler line. In addition, the revised publication [10] acknowledges an error in the ordering of 217 GHz beam transfer functions that leads to changes in the 217 GHz spectra by a few μK^2 for $\ell > 2000$. To what extent this is related to the excess noted here is difficult to assess. The corrected spectra are not publicly available, and this may be compensated in the likelihood analysis by a shift in the parameters of the foreground model.
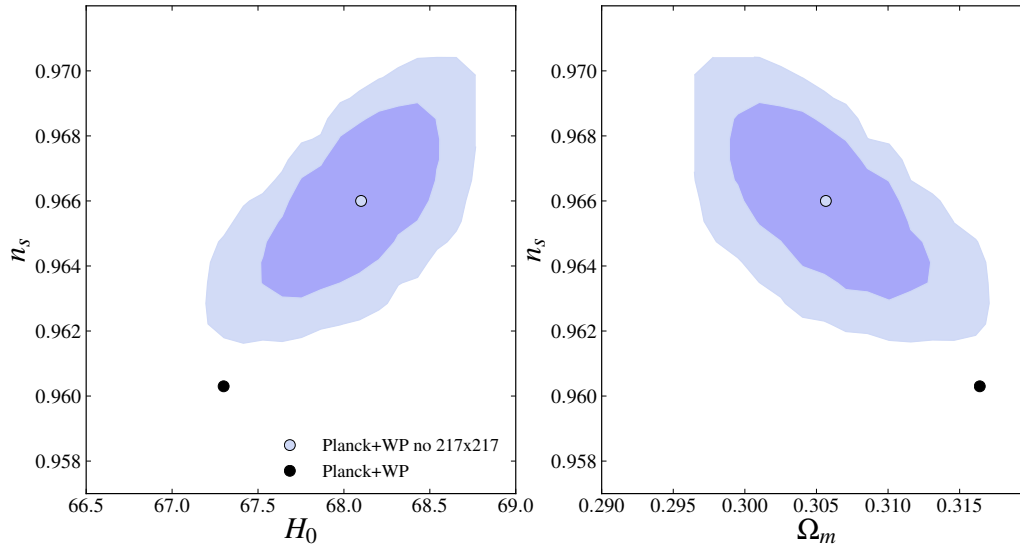
FIG. 1: Means for n_s, Ω_M and H_0 derived from the publicly available Planck likelihood code (black) and without the 217×217 data (gray), both for the Planck+WP data set. The contours indicate the regions that contain 68 and 95% of our 500 simulations with 217×217 spectra drawn from the conditional probability (1).

decreases the errors by $\sim 15\%$, but shifts the resulting mean values for H_0, n_s and $\Omega_c h^2$ by about $1\,\sigma$.[2] Motivated by these shifts, we have explored whether the reported 217×217 power spectra are consistent with the other spectra. To quantify magnitude of shifts that are expected when adding the 217×217 data, we have performed simulations. We use the inverse covariance matrix in the CAMspec likelihood code, $\mathcal{D}$, to derive the conditional probability for 217×217 power spectra given the measured 100×100, 143×143, and 143×217 power spectra

$$p(Y_\alpha | Y_j) \;=\; \sqrt{\det\left(\frac{\mathcal{D}_{\alpha\beta}}{2\pi}\right)} \times \exp\left[-\frac{1}{2}(Y_\alpha - \langle Y_\alpha\rangle)\mathcal{D}_{\alpha\beta}(Y_\beta - \langle Y_\beta\rangle) \right] \qquad \text{with} \qquad \langle Y_\alpha\rangle = -\mathcal{D}_{\alpha\beta}^{-1}\mathcal{D}_{\beta j} Y_j\,. \qquad (1)$$

Here Y_α is the difference between the 217×217 spectrum and the fiducial model, Y_j are the difference between the 100×100, 143×143, and 143×217 spectra and their fiducial models, and $\mathcal{D}_{\alpha\beta}^{-1}$ denotes the inverse of the $217 \times 217 \times 217 \times 217$ block of the inverse covariance matrix. We then draw 217×217 spectra from this distribution, combine them with the measured 100×100, 143×143, 143×217 spectra and derive the cosmological parameters for each simulation. The result for 500 simulations is shown in Figure 1. Uncertainties in the beams are not included in the simulations, and the details depend somewhat on whether means or best-fits are considered, but it is safe to say that the shifts are somewhat larger than expected. The different frequencies agree very well when the multipole range is restricted to $\ell < 1500$ and an analysis restricted to this range leads to values of cosmological parameters consistent with WMAP9+ACT. In [26], the Planck team identified a feature near $\ell \simeq 1800$ with a significance of $2.4 - 3.1\sigma$. Replacing the data in this range by simulations, this feature does not, however, lead to significant shifts in cosmological parameters. This is partly because it is only present in the 217×217 data, and partly because it is hard to accommodate such a feature by adjusting parameters in ΛCDM. As was already noted by the Planck team (see e.g., Figure B.3 in) [10], a comparable shift is observed when removing data for $\ell > 2000$ from the fit. It is tempting to conclude that the excess is responsible for the observed shift, but it should be kept in mind that removing the $\ell > 2000$ data from the fit changes the weighting so that other ranges of multipoles may also be important to understand the origin of these shifts.

Another way to test the consistency between the different spectra is to show the prediction for the 217×217 spectra

---

[2] In comparing the numbers in Table I one should keep in mind that the Planck analysis assumed the sum of neutrino masses to be $0.06\,eV$, while this was set to zero in previous analyses (such as [11]). As shown in [10], this leads to a small shift in parameters. To facilitate comparison with the Planck results, we set the sum of the neutrino masses to $0.06\,eV$ as well.
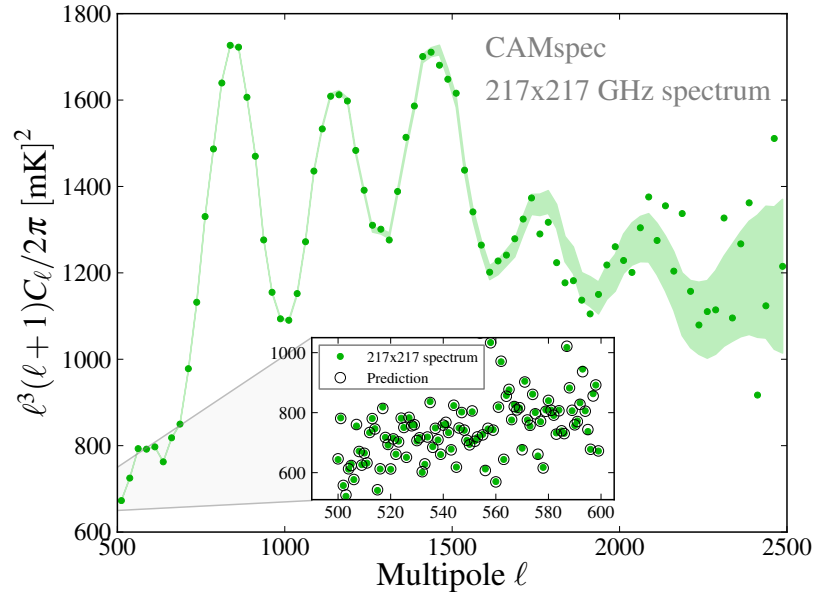
FIG. 2: Predicted versus observed power spectra: This figure shows the difference between the published 217×217 spectrum binned with $\Delta\ell = 25$ (points) and the spectrum predicted from the published Planck 100×100, 143×143, and 143×217 spectra (filled band indicates 68% CL). Note that the points are systematically below the model for $1700 < \ell < 1900$ and above the model for $2100 < \ell < 2400$. In the boxed insert, we show the predicted spectrum and observed spectrum for each multipole between $500 < \ell < 600$ where predicted and measured spectra agree remarkably well.

together with the measured spectra. This is significantly easier because both the mean and the variance are known analytically from (1). Figure 2 shows this comparison of the predicted 217×217 spectra with the observed spectra. There are two noticeable deviations: the points are systematically low at $\ell = 1800$ as discussed, and systematically high at $\ell > 2000$, a multipole range where a number of the 217 GHz detectors fail their null tests [25]. The $\ell = 1800$ feature is suggestively near one of the resonances of the 4K cooler line [25]; however, this cooler line should have been removed in the HFI processing.[3]

III. PLANCK SPECTRUM REVISITED

Motivated by the discrepancies discussed in §II, we have performed an analysis based on the publicly available Planck data. Since the Planck team has only released survey and halfring maps rather than the detector set maps used in their power spectrum analysis, we cannot directly reproduce their analysis (see Section V C for more discussion on the halfring maps). On the one hand this means we are using a subset of the Planck data in the power spectrum measurements, and the error bars (for the same $f_{\rm sky}$) are larger in our analysis. On the other hand, our approach of using only survey cross-spectra is much more robust to systematics that are common between detectors observing the sky at the same time. In fact, in the analysis of ground-based CMB experiments, most analyses use only cross-spectra of maps of the sky observed at different times, e.g. [27] as these are less prone to common-mode systematics.

In order to reduce the cosmic variance errors in the power spectrum (and obviate the effects of using a smaller set of cross-spectra), we use more data by analyzing a larger fraction of the sky. This is possible because of Planck's wide frequency coverage which allows a much more aggressive approach to removing foregrounds than was possible in

---

[3] At the time this work was submitted, the origin of the feature had not been established. In the revised *Planck* publication [10] it was identified as a systematic associated with the incomplete removal of the time-variable electromagnetic interference between the 4K cooler electronics and the read-out electronics from the time-ordered data. Furthermore, the revised publication mentions an error in the ordering of beam transfer functions causing a change in the 217 GHz spectrum by a few (μK^2) [10], just the right amount to account for the systematic difference in the spectra at $\ell > 2000$.
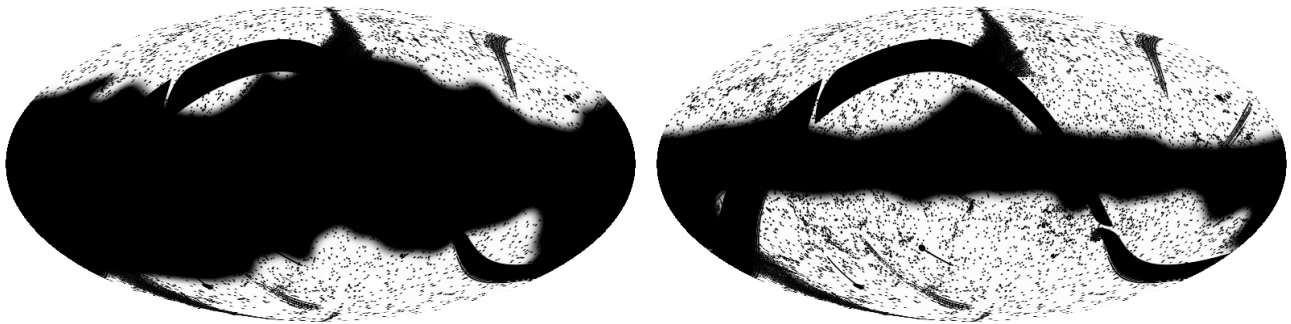
FIG. 3: This figure shows the more conservative mask used in the Planck analysis in which foregrounds are modeled, SA24 (left) and the less conservative mask used in our main analysis, SA47 (right). These masks are a product of a point source mask, a mask that excludes pixels observed only in a single survey, and galactic masks with $f_{\rm sky} = 35\%$ for SA24 and 70% for SA47. With the SA24 mask, there is 24.3% of the sky available for analysis, with the SA47 mask there is 46.8% of the sky available for analysis.

small-scale experiments such as ACT [6] and SPT [28]. In our analysis, we make use of the publicly available survey maps at 100, 143, 217, 353 and 545 GHz for the power spectrum measurement, and use the 857 GHz data to construct galactic masks.

The galactic masks are obtained by thresholding the 857 GHz map after smoothing with a FWHM = $10°$ Gaussian. Our main analysis is based on a galactic mask with $f_{\rm sky} = 70\%$. To show the robustness of our cleaning procedure, we also present results based on galactic masks with $f_{\rm sky} = 35\%$, $f_{\rm sky} = 56\%$, $f_{\rm sky} = 65\%$, and $f_{\rm sky} = 75\%$. For comparison with the Planck analysis, we also generate galactic masks with $f_{\rm sky} = 35\%$ and $f_{\rm sky} = 56\%$ by thresholding the 353 GHz map, again after smoothing with FWHM = $10°$ Gaussian. All galactic masks are then apodized as described in [9] by smoothing with FWHM = $5°$ Gaussian, subtracting 0.15 from each pixel, setting pixels with negative values to zero, and dividing the value of each pixel by 0.85.

To make our point source masks, we use the masks provided in `HFI_Mask_PointSrc_2048_R1.10.fits`, which mask point sources detected at $5\,\sigma$ in HFI channels as described in [29]. For the analysis in which foregrounds are modeled at the level of the power spectrum, as well as for cleaning with 353 GHz, we use the union of these masks from 100 to 353 GHz. For cleaning with 545 GHz and hybrid cleaning we use the union of the masks for 100 to 545 GHz. We apodize these two union masks with a Gaussian with FWHM = $30'$. We also mask the pixels that are not observed in both seasons and apodize them with a Gaussian with FWHM = $30'$.

The final masks used in the analysis are the product of galactic, point source, and survey mask. Two masks are shown in Figure 3, the more conservative mask leaves 24.3% of the sky for analysis, the less conservative mask leaves 46.8% of the sky for analysis. We refer to these apodized survey masks based on galactic masks with $f_{\rm sky} = 35\%$ and 70% as SA24 and SA47. Similarly, we refer to the mask based on the galactic masks with $f_{\rm sky} = 56\%$, 65% and 75% as SA38, SA44, and SA50, respectively.

To test for stability we have used various different degrees of apodization with negligible effect on cosmological parameters. Since we only use 545 GHz data for cleaning, our point source mask is very conservative. We have also performed analyses in which 545 GHz point sources are not masked and find that they lead to virtually identical cosmological parameters. In addition, we have also estimated cosmological parameters from maps that were filtered to minimize mode coupling and have found no significant shifts. The robustness of the cosmological parameters derived from sky fractions varying from 24% to 50% indicates that CO is not a significant contaminant for our masks. We have also checked this directly using CO maps provided by Planck as well as CO maps made based on the observation that the 100 GHz HFI bandpass includes the CO line while the 94 GHz WMAP W-band does not.

Using the high frequency maps (343 and 545 GHz), we produce two dust-cleaned maps for each of the intermediate frequency survey maps (100, 143 and 217 GHz). We find the coefficient that minimizes the high ℓ angular power spectrum of the clean maps

$$T_{ij}^{clean} = (1 + \alpha_{ij})T_i - \alpha_{ij}T_j , \qquad (2)$$

at high galactic latitude. As an example, Figure III shows the coefficient, $\alpha_{217,353}$ that minimizes a linear combination of the 217 and 353 GHz maps and Table II lists the coefficients used in the map cleaning. For 100 GHz, we extract them from the multipole range $1000 < \ell < 1200$, for 143 GHz from $1500 < \ell < 2000$, and for 217 GHz from $2000 < \ell < 2500$. Figure III shows that the dependence of the cleaning coefficient on multipole is weak so that the choice of ℓ-range has a very mild effect. Furthermore, the minimum is relatively broad and small changes in cleaning
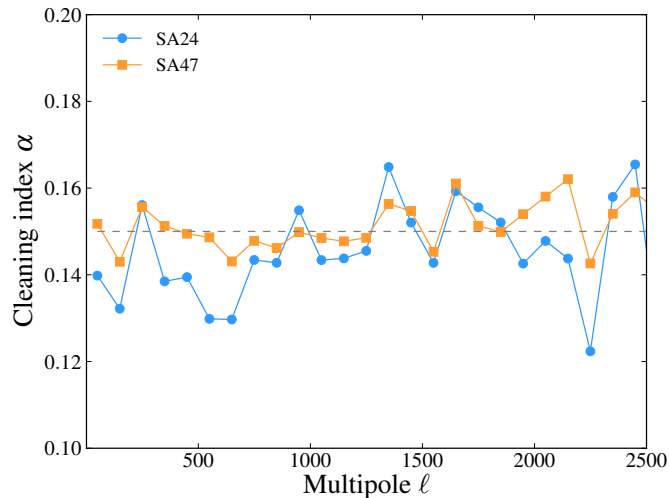
coefficients do not affect the analysis.

FIG. 4: This figure shows the amplitude of the optimal coefficient to minimize foregrounds based on minimizing $((1+\alpha)T_{217} - \alpha T_{353})^2$ as a function of multipole number ℓ and sky cut. The blue dots are for mask SA24 and the orange squares for SA47. The dashed line shows the value chosen for map cleaning which was fixed to minimize the extragalactic foregrounds. There is no significant variation in the cleaning coefficient with multipole or sky cut.
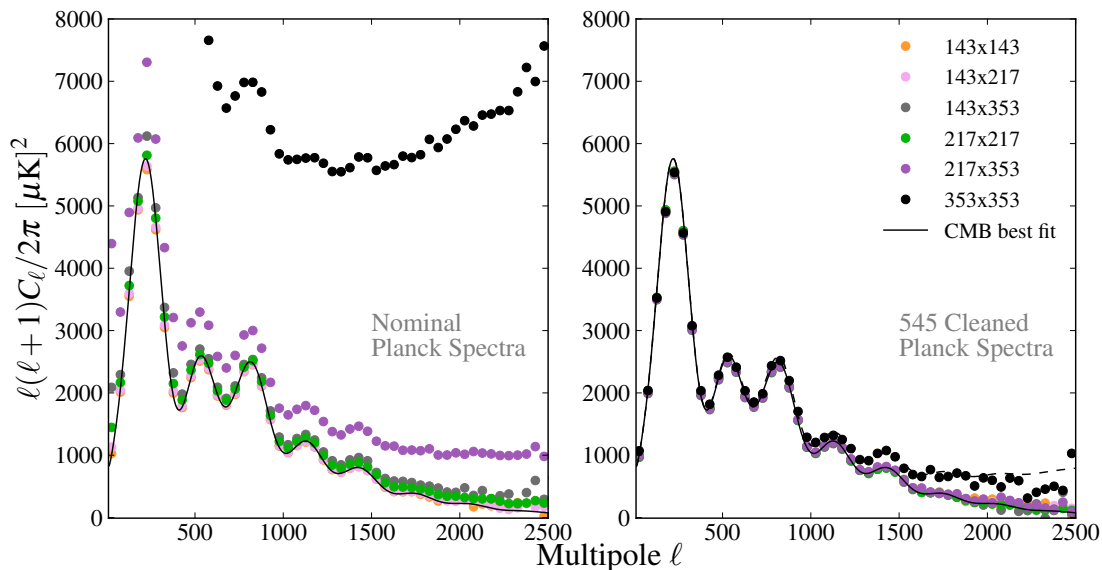

FIG. 5: Planck spectra before and after foreground cleaning for mask SA47. *Left panel:* Planck spectra from the uncleaned maps, masked to remove point sources and galactic emission. *Right panel:* Foreground-cleaned Planck spectra using the 545 GHz data to clean the maps used in the cosmological analysis. The solid line shows the best-fit CMB spectrum while the dashed line indicates the residual Poisson foreground emission after cleaning with an amplitude of 458 $(\mu K)^2$ at $\ell = 2000$, as shown in Figure 6.

Cleaning with 545 GHz removes the extragalactic dusty sources very effectively. Figure 5 compares the 'raw' Planck spectra computed for the SA47 sky cut with the 545-cleaned spectra. The figure shows that the 545 cleaning is able to reduce the foreground contribution at 353 GHz by about a factor of 15 (in power) at $\ell \sim 1800$. Using the double

difference technique presented in [9], we estimate the galactic contribution to the foregrounds at 353 GHz in this ℓ-range to be around $1000\,\mu K^2$. Cleaning with 545 GHz removes this contribution almost entirely with a residual of $\lesssim 10\,\mu K^2$. This implies that more than 90% of the contribution of dusty sources is removed. Figure III shows the level of residual extragalactic point sources based on the difference between the 545-cleaned map power spectrum and our best-fit CMB spectrum. The plot shows that the residual is well fit by a Poisson term with no evidence for any clustered galaxy term at either 217 GHz or 353 GHz. We can use the 217×353 and 353×353 spectra to estimate the

TABLE II: Coefficient α_{ij} used in the cleaning procedure for mask SA47

Template	353	545
100	0.008	0.001
143	0.03	0.002
217	0.15	0.0085
353	-	0.064

residual level of dusty galaxy point source contributionin the 217×217 spectrum. We assume that the flux density for these sources obeys a power law with constant spectral index from 217 GHz through 545 GHz, so that

$$C_\ell^{dust,217\times353} = (C_\ell^{dust,217\times217} C_\ell^{dust,353\times353})^{1/2} . \tag{3}$$

This leads to $\ell(\ell+1)C_{2000}^{PS}/2\pi \approx 4\,\mu K^2$ for the 217×217 spectrum after subtraction with a 545 GHz template. The difference between the cleaned power spectrum and the CMB-only spectrum that best fits the 545 GHz-cleaned data, is fit by a residual point source amplitude of around 17 $(\mu K)^2$, consistent with the expected additional contribution from synchrotron sources. For our 353 GHz maps, we can also estimate the residual level of dusty source contamination from Equation (3). For the 217×217 spectrum, we find $\ell(\ell+1)C_{2000}^{PS}/2\pi \lesssim 1\,\mu K^2$, consistent with estimates based on an extrapolation assuming a power law.
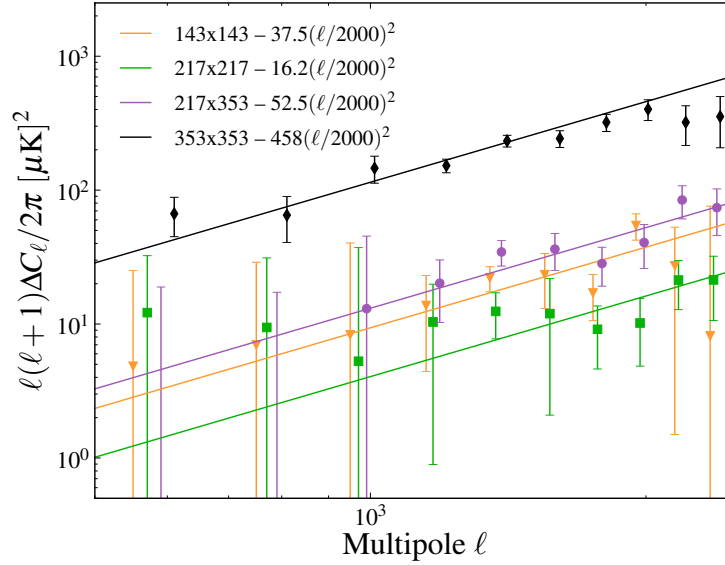

FIG. 6: This figure shows the difference between the cleaned power spectra shown in Figure 5 and the best-fit CMB spectrum to the 545 GHz-cleaned data. The solid line shows a fit to this residual of a point source contribution of 458 $(\mu K)^2$ at $\ell = 2000$ for 353×353 and 52.5 $(\mu K)^2$ for 217×353. If the emission spectra of the dusty galaxies scale as a power law over the 217-545 GHz frequency range, then the residual power in 217×217 spectra due to dusty galaxies is 4 $(\mu K)^2$ at $\ell = 2000$. The fit shown in the plot is for a 16.2 $(\mu K)^2$ contribution at 217×217, consistent with the expected additional signal due to synchrotron sources. The fit shown for the 143×143 spectrum is 37.5 $(\mu K)^2$.

Since the spectrum of the galactic dust is close to that of the extragalactic dust, foreground cleaning also significantly

reduces the galactic dust contribution in our cleaned maps. We estimate the residual galactic emission using the double difference technique presented in [9], and find that the residual galactic contribution is less than $\sim 1\,\mu\text{K}^2$, both for cleaning with 353 and 545 GHz. While the 353 GHz cleaning is slightly more effective at removing both the extragalactic clustered dust contribution and the galactic foregrounds, the cost of this cleaning procedure is a 25% increase in the noise in the cleaned maps.

For our analysis, we compute the cross-spectra of the 353 GHz-cleaned maps with the 545 GHz-cleaned maps. This hybrid approach has the advantage of nearly halving the additional noise cost associated with using the high-frequency maps and being insensitive to the details of the 353 GHz and 545 GHz maps. We will focus on results from the hybrid cleaned spectra using the SA47 sky cut, but we have also computed cosmological parameters for a number of other sky cuts as well as for 353 GHz and 545 GHz cleaned spectra to check for stability. We show a subset of the various approaches in Figure 9.

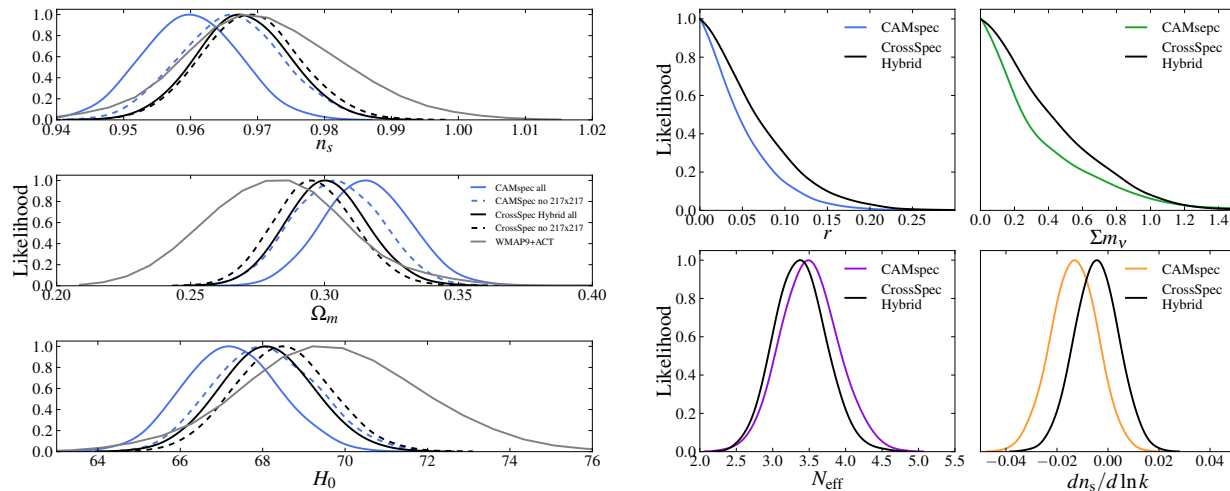## IV. COSMOLOGICAL PARAMETERS USING CLEANED SPECTRA

FIG. 7: Constraints on key parameters in the ΛCDM model and extensions in the presence of high-frequency foreground cleaning. *Left panel:* The top, middle and bottom panels show the marginalized one-dimensional likelihoods for the scalar spectral index, n_s, the matter density Ω_m and the Hubble constant H_0 in the ΛCDM model. The solid blue line is the standard Planck result for the CAMSpec likelihood including the 100×100, 143×143, 217×217 and 143×217 spectra. The dashed blue line shows the results when the 217×217 spectra are not used; these correspond to results presented in Figure B3 of [10]. The solid and dashed black lines show the same for the cleaned spectra presented here. *Right panel:* Constraints on the tensor-to-scalar ratio (top left panel) and mass of the neutrino (top right panel) are weakened with cleaning of the spectra, and N_{eff} (bottom right hand panel) shifts to values slightly more consistent with three neutrino species. The cleaned spectra do not show a preference for running of the scalar spectral index.

For the estimate of cosmological parameters, we use Planck's 'clik' likelihood code. We leave the Commander and lowlike likelihood unchanged, but modify CAMspec to accomodate the changes in our analysis. Our basic approach follows the procedures outlined in Planck papers XV and XVI as closely as possible. We replace the Planck team's 100×100, 143×143, 143×217 and 217×217 spectra with the 'hybrid cleaned' spectra that we have computed from the publicly available maps using the procedures described in §III. We compute the covariance matrices for the spectra using the same approximations described in Appendix A of Planck paper XV with appropriate modifications to take into account the noise in the 353 GHz and 545 GHz maps used in the cleaning. Since the noise is colored, noise corrections are required for an accurate covariance matrix. We measure these corrections by fitting the Planck noise model to noise spectra obtained from survey differences. As fiducial models for the covariance matrices, we use the best-fit from a run based on a covariance matrix for the same masks and cleaning procedure in which they were taken to be CMB only. We retain the modeling of extra-galactic foregrounds used in CAMspec and thus the nuisance parameters [9] and use the conventions and units given there.

We then use CAMB [30] and CosmoMC [31] to derive constraints on cosmological parameters for the Planck+WP

data set with our likelihood. We find best-fit cosmological parameters that are closer to pre-Planck values than the results in [10]. Figure 7 shows the marginalized one-dimensional likelihoods for the three parameters in the standard ΛCDM model which showed significant shifts in the recent Planck results relative to previous analyses. The constraints using the cleaned spectra (indicated by the blue lines in Figure 7) are more consistent with previous results, such as those from ACT [6], shown in gray. The most notable shifts are along a modest degeneracy line between n_s, H_0 and Ω_m:[4]

TABLE III: Constraints on the ΛCDM model parameters in the cleaning procedure compared to the nominal Planck parameters.

Parameter	Planck constraint	Hybrid cleaning constraint ($f_{sky} = 0.47$)
Primary Parameters		
$\Omega_b h^2$	0.02204 ± 0.00028	0.02197 ± 0.00026
$\Omega_c h^2$	0.1199 ± 0.0026	0.1170 ± 0.0025
θ_A	1.04131 ± 0.00062	1.04066 ± 0.00056
τ	0.089 ± 0.013	0.090 ± 0.013
n_s	0.9604 ± 0.0073	0.9686 ± 0.0069
$\ln(10^{10} A_s)$	3.088 ± 0.025	3.082 ± 0.025
Derived Parameters		
H_0	67.3 ± 1.2	68.0 ± 1.1
Ω_m	0.316 ± 0.016	0.302 ± 0.015
σ_8	0.829 ± 0.016	0.818 ± 0.012
Secondary Parameters		
A_{100}^{PS}	171 ± 60	170 ± 43
A_{143}^{PS}	54 ± 13	59 ± 13
A_{217}^{PS}	107 ± 17	17.5 ± 6.6
A_{143}^{CIB}	8.1 ± 5.4	7.5 ± 5.1
A_{217}^{CIB}	28.9 ± 7.4	1.6 ± 1.5
A^{tSZ}	5.2 ± 2.8	4.5 ± 1.8
$r_{143\mathrm{x}217}^{\mathrm{PS}}$	0.883 ± 0.079	0.94 ± 0.055
$r_{143\mathrm{x}217}^{\mathrm{CIB}}$	0.429 ± 0.221	0.71 ± 0.25
γ_{CIB}	0.53 ± 0.13	0.81 ± 0.19
c_{100}	1.00058 ± 0.00040	1.00259 ± 0.00044
c_{217}	0.99638 ± 0.0014	0.99591 ± 0.00083
ξ_{tSZxCIB}	0.47 ± 0.29	0.54 ± 0.29
A_{kSZ}	4.5 ± 2.9	4.0 ± 2.7

- **the spectral index** n_s, is about $1\,\sigma$ higher in our analysis with mean 0.9686 ± 0.0069, still significantly different from $n_s = 1$.

- **the Hubble constant** $H_0 = 68.0 \pm 1.1$ km s^{-1}Mpc^{-1}, shifts upwards from the best-fit Planck value by $0.6\,\sigma$, within $1\,\sigma$ of the value inferred from the WMAP9 data, $H_0 = 70.0 \pm 2.2$ km s^{-1}Mpc^{-1} and within $2\,\sigma$ of published local estimates of the Hubble constant, 73.8 ± 2.4 km s^{-1}Mpc^{-1} [12] and $74.3 \pm 1.5 \pm 2.2$ km s^{-1}Mpc^{-1} [13]. Our recomputed value is even closer to the recent re-evaluation based on a new distance to NGC 4258, 70.6 ± 3.3 km s^{-1}Mpc^{-1} [32], a difference of only $0.8\,\sigma$ and within $1.8\,\sigma$ of the analysis based on NGC 4258, Cepheids in the LMC and the Milky Way presented there which yielded 72.5 ± 2.5 km s^{-1}Mpc^{-1}. Our value for the Hubble

---

[4] In all comparisons, we will use the standard deviation of the experiment with the larger uncertainty when stating that one measurement is within $x\,\sigma$ of the other.
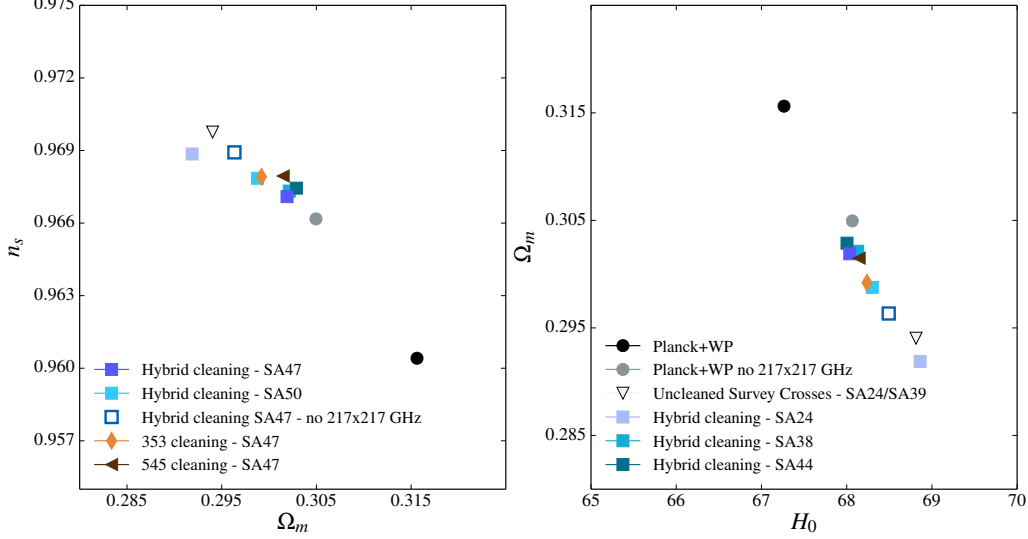
FIG. 8: Constraints in the $\Omega_m - n_s$ plane (left) and $H_0 - \Omega_m$ plane (right) for various cleaning strategies and datasets, compared to the Planck results. The circles show results obtained with the nominal Planck data, the squares show results from the hybrid cleaning procedure, the diamond are obtained when only cleaning with the 353 GHz data, and the triangle when using the 545 GHz data to clean the lower frequencies. For comparison, the results are shown for the season cross-spectra without additional cleaning (upside-down triangle). The cosmological results are robust to a change in the cleaning procedure. The uncleaned survey crosses use the combination of masks used by Planck, modified to mask pixels observed in only one survey. We refer to them as SA39 for 100 GHz and SA24 for 143 and 217 GHz.

constant is also more consistent with gravitational lensing timing measurements [33]. Of course, it should be kept in mind that even after a shift by 0.6 Planck σ the CMB in the context of ΛCDM still indicates a lower value of H_0 than the astonomical measurements.

- **the matter density** Ω_m **and** σ_8 are about 1σ lower. We find $\Omega_m = 0.302 \pm 0.015$ compared to Planck's value of $\Omega_m = 0.316$, and $\sigma_8 = 0.818 \pm 0.012$ compared to $\sigma_8 = 0.829$ reported by Planck. The lower matter density and σ_8 also imply a lower number of rich clusters which determine a combination that scales as $\sigma_8(\Omega_m/0.27)^{0.3}$. The Planck team reports an amplitude of 0.87 ± 0.02 [10], $\sim 3\sigma$ discrepant from the value inferred from the Planck SZ cluster measurement: 0.79 ± 0.01 [21]. Our analysis leads to the constraint $\sigma_8(\Omega_m/0.27)^{0.3} = 0.84 \pm 0.02$ lowering the tension to $\sim 2\sigma$, but not eliminating it entirely. Measurements of the X-ray cluster-SZ cross-correlation yield the constraint $\sigma_8(\Omega_m/0.3)^{0.26} = 0.797 \pm 0.015$ [23]. We find $\sigma_8(\Omega_m/0.3)^{0.26} = 0.818 \pm 0.019$, a difference of only 1σ. The normalization of the local mass function determined from X-ray cluster data yields $\sigma_8(\Omega_m/0.25)^{0.47} = 0.813 \pm 0.013$ [22]. We find $\sigma_8(\Omega_m/0.25)^{0.47} = 0.892 \pm 0.028$, still in tension with this measurement at 2σ after accounting for systematics mentioned in [22]. The CFHTLens analysis finds $\sigma_8 = 0.799 \pm 0.015$, within 1σ of our measurement, but finds $\Omega_m = 0.27 \pm 0.010$ about 2σ lower than our measurement. Some of these results are summarized in Figure 9.

For the cleaned spectra, the best-fit values of the foreground parameters change, as shown in Table III. In general we expect the amplitudes of foreground parameters such as the point sources amplitudes at 217 GHz to reduce dramatically, where the amplitudes of the CIB at 143 and 217 GHz are consistent with a non-detection. The amplitude of the CIB sources at 217 GHz is also reduced from $A_{217}^{CIB} = 27 \ (\mu K)^2$ to $A_{217}^{CIB} < 10 \ (\mu K)^2$ at 95% confidence, and the upper limit at 143 GHz also slightly reduces in amplitude.

In the Planck team analysis [10], the cosmological parameters change when the analysis excludes the 217×217 spectrum, as shown in Figure 7. To a smaller extent this trend continues even when using cleaned data. The shifts are now roughly consistent with expectations based on simulations, but they could nevertheless indicate a remaining systematic in the 217×217 data that is not removed with the cleaning procedure. We note that the best-fit parameters obtained in our hybrid cleaning analysis are very close to the best-fit values for the Planck team analysis without the 217×217 power spectrum.

Using the 353 GHz and 545 GHz hybrid cleaning on the publicly available maps, we have also recomputed the
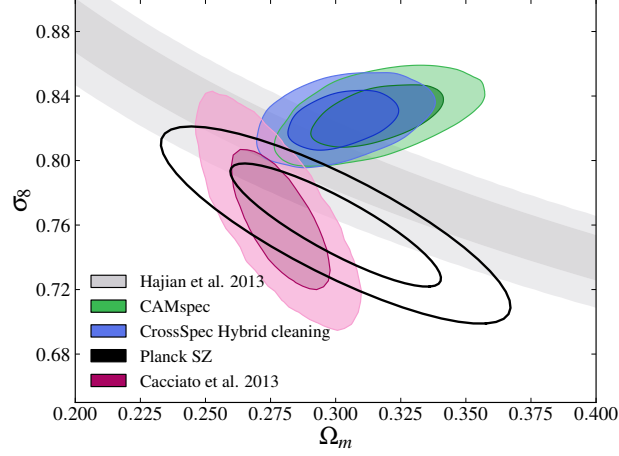
FIG. 9: Constraints on σ_8 for the hybrid cleaning method (in blue), in comparison to the constraints from the Planck CMB constraints (green filled contours [10]), Planck SZ clusters (black unfilled contours [17]), constraints on the SZ emission from cross correlation of CMB maps and galaxy cluster catalogs (grey band [23]) and from a combination of galaxy clustering and lensing (pink filled contours [24]).
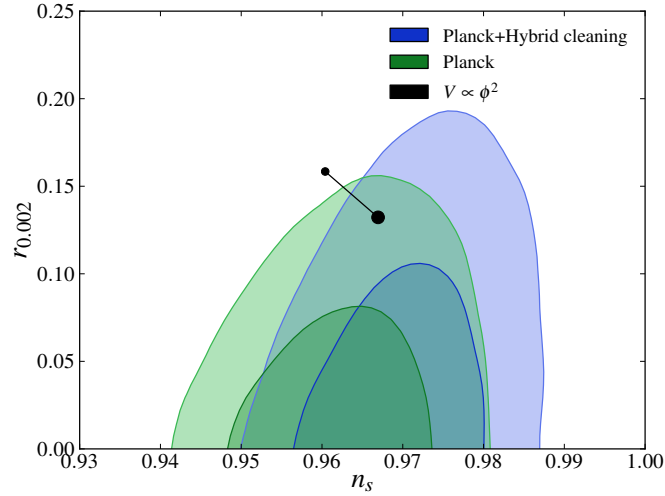

FIG. 10: Constraints on $n_s - r$ plane. The black dots indicated the predicted values for $m^2\phi^2$ inflation with 50 and 60 e-folds between reheating scale and the horizon scale today.

best-fit parameters for several extensions of the standard ΛCDM model. Our re-analysis, shown in Figure 7, finds no evidence for new physics in contrast with [28]: the mean of the posterior for the effective number of relativistic species is 3.34 ± 0.35, within ~ 1 σ of the standard value, and a best-fit point of $N_{\rm eff} = 3.13$. In addition, there is no evidence for neutrino mass, and the best-fit does not provide evidence for the running of the spectral index, $dn_s/d\log(k) = -0.0046 \pm 0.0085$. Figure 10 shows the recomputed constraints on the $n_s - r$ plane: the $m^2\phi^2$ model lies within the 95% confidence region; however, the data favors models with lower values of r and larger values of n_s.

V. WHY DOES THIS ANALYSIS YIELD DIFFERENT COSMOLOGICAL PARAMETERS?

Our analysis of the publicly available Planck data has led to parameters that are different from those found by the Planck team [10] by about $1\,\sigma$. In this section we summarize what might be responsible for them.

A. Not Due to the Large f_{sky}

TABLE IV: Table of mean values of parameters from hybrid cleaning with different values of f_{sky}.

	$f_{sky} = 0.38$	$f_{sky} = 0.44$	$f_{sky} = 0.47$	$f_{sky} = 0.50$
$\Omega_c h^2$	0.1174	0.1173	0.1170	0.1167
n_s	0.9681	0.9683	0.9685	0.9683
h	0.681	0.680	0.680	0.682
$100\,\Omega_b h^2$	2.197	2.197	2.197	2.204
$\log(10^{10} A_s)$	3.087	3.082	3.082	3.082
τ	0.092	0.090	0.090	0.091
$-2\ln\mathcal{L}_{\mathrm{CAMspec}}$	7529.96	7530.04	7542.45	7626.79
$-2\ln\mathcal{L}_{\mathrm{Commander}}$	-8.14	-8.31	-8.32	-8.22
$-2\ln\mathcal{L}_{\mathrm{lowlike}}$	2014.60	2014.60	2014.57	2014.70

We work with survey cross-spectra rather than the detector set spectra used by the Planck team. As discussed, this means we have less data available for the same f_{sky}. Because we are cleaning the maps, we can easily increase the fraction of the sky used in the analysis to use more data. This increase in f_{sky} may have led to shifts in cosmological parameters. Here we show that the computed power spectra and the best-fit parameters are insensitive to the fraction of the sky used for the analysis. There is no statistically significant difference between the SA24 and SA47 power spectra even when binned with $\Delta\ell = 200$. Furthermore, as shown in Figure 8 and in Table IV, the cleaned cross-season power spectra and best-fit parameters are consistent for a large range of sky cuts. This suggests that there is minimal residual galactic contribution after cleaning the spectra with the 353 GHz and 545 GHz maps. This is confirmed by measurements of the residual galactic contribution based on the double difference method described in [9].

Table IV also justifies the choice of sky fraction used in our main analysis. On the one hand we would like to use as much of the sky as possible. On the other hand we know that our foreground model will eventually break down. We interpret the sharp increase in $-2\ln\mathcal{L}_{\mathrm{CAMspec}}$ between the third and fourth column as a signal that this occurs for $f_{\mathrm{sky}} > 47\%$. The table shows that $-2\ln\mathcal{L}_{\mathrm{CAMspec}}$ is stable for galactic masks with $f_{\mathrm{sky}} \leq 47\%$ so that our analysis is based on the mask with the largest f_{sky} for which we know that the foregrounds are well modeled. Notice, however, that the cosmological parameters do not yet shift significantly for the mask with $f_{\mathrm{sky}} = 50\%$ corresponding to a galactic mask with $f_{\mathrm{sky}} = 75\%$.

B. Not Due to the Cleaning Procedure

In the Planck team analysis foregrounds are modeled at level of the power spectrum and the amplitudes of the various templates are marginalized over, with the exception of diffuse galactic emission, for which a template is subtracted from the measured spectra. In our main analysis we clean the maps, which allows us to use significantly larger fractions of the sky. This cleaning could itself introduce systematics and be responsible for shifts in cosmological parameters. To minimize such systematics, our main analysis relies on a hybrid cleaning method based on two sets of maps cleaned with 353 GHz and 545 GHz so that no 353×353 or 545×545 spectra are used. In table V, we compare cosmological parameters derived from this hybrid cleaning as well as cleaning with 353 GHz and 545 GHz only, all based on the mask SA47. We see that the different ways of cleaning the maps lead to very consistent results, suggesting that our cleaning does not introduce systematics that lead to significant shifts in cosmological parameters. For comparison, we also present an analysis applying Planck's foreground model to season cross-spectra. For these uncleaned survey crosses, we use the combination of masks used by Planck, modified to mask pixels observed in only one survey. We refer to them as SA39 for 100 GHz and SA24 for 143 and 217 GHz. As shown in Figure 8, for similar

$f_{\rm sky}$ our cleaning also leads to results consistent with those found by applying Planck's foreground model to season cross-spectra.

TABLE V: Table of mean values of parameters based on various cleaning procedures.

	353 GHz	545 GHz	Hybrid cleaning
$\Omega_c h^2$	0.1165	0.1171	0.1170
n_s	0.9681	0.9675	0.9685
h	0.682	0.680	0.680
$100\,\Omega_b h^2$	2.202	2.200	2.197
$\log(10^{10} A_s)$	3.080	3.084	3.082
τ	0.089	0.091	0.090
$-2\ln\mathcal{L}_{\rm CAMspec}$	7590.66	7560.26	7542.46
$-2\ln\mathcal{L}_{\rm Commander}$	-8.22	-7.79	-8.33
$-2\ln\mathcal{L}_{\rm lowlike}$	2014.66	2014.66	2014.57

To check for potential systematics at the level of the power spectra, we use Equation 1 to predict the 217×217 spectrum based on the spectra at other frequencies for the different approaches we used. The result is shown in Figure 11. The trend seen in Figure 2 with observed data systematically below the predicted band for $1700 < \ell < 1900$ and above the band for the range $2100 < \ell < 2400$ is not seen in any of the spectra computed from season cross-spectra. In addition, the panels which show the cleaning procedures highlight the reduction in the error bars due to increased $f_{\rm sky}$ possible when applying the cleaning procedure.

Finally, we test that the cleaning is robust to removing the CIB modeling. From the full set of parameters presented in Table III, we note that the CIB amplitude at 217 GHz are consistent with zero in the cleaned spectra. We find that the cosmological parameters do not shift by more than $0.2\,\sigma$ when removing the CIB terms completely and setting $A_{217}^{\rm CIB}$ and $\gamma_{\rm CIB}$ to zero.

C. Mostly due to the Detector Set Spectra or Regions Observed Only Once

The spectra used in the Planck high-ℓ likelihood were made using data from individual detector sets. While these spectra have reduced scatter from the many cross correlations possible between detector sets, they are also more likely to be prone to any systematic effect correlated between detectors, such as the 4K cooler line and the notch filter that produces echoes in the map (see Section 3.6 in [25]). In contrast, the publicly available Planck maps are made by

TABLE VI: Table of mean values of parameters from the nominal Planck data.

	Planck Team	Uncleaned Cross-Season	Half-Ring Survey $1 \cap 2$	Half-Ring Survey $1 \cup 2$
$\Omega_c h^2$	0.1199	0.1162	0.1173	0.1186
n_s	0.9603	0.9698	0.9655	0.9595
h	0.673	0.688	0.682	0.677
$100\,\Omega_b h^2$	2.204	2.214	2.197	2.202
$\log(10^{10} A_s)$	3.088	3.084	3.087	3.084
τ	0.089	0.091	0.092	0.089
$-2\ln\mathcal{L}_{\rm CAMspec}$	7795.11	7462.72	7715.93	7590.70
$-2\ln\mathcal{L}_{\rm Commander}$	-6.96	-7.68	-7.69	-6.63
$-2\ln\mathcal{L}_{\rm lowlike}$	2014.44	2014.41	2014.51	2014.41

combining the data of all detectors in a given channel in the first two Planck observational seasons. The cross-spectra
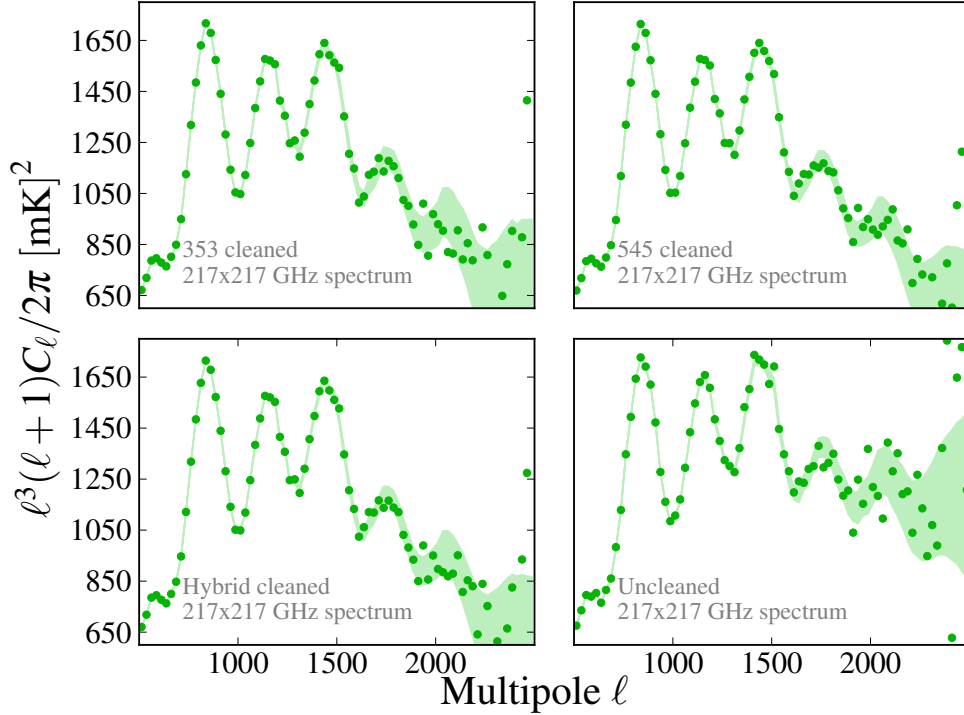
FIG. 11: Predicted versus observed 217×217 spectrum. The shaded bands show the predicted envelope for the 217×217 spectrum from the 100×100, 143×143 and 143×217 spectra. The points show the observed 217×217 spectrum in each case. By comparing the predicted spectrum from the cleaning done using the 353 GHz spectrum, we see that the data are consistent with the prediction in the $\ell > 1500$ region. The same is true for the hybrid cleaning procedure. The prediction is based on equation (1) and the best-fit foreground spectrum.

computed from these season maps have larger noise than the detector set cross-spectra but are less sensitive to such systematics. A comparison between the detector set spectra and the season cross-spectra is shown in Figure 12.

As shown in table VI, the cosmological parameters derived from the detector set spectra are systematically different from the survey cross-spectra using Planck's treatment of foregrounds. The parameters derived from the survey cross-spectra are closer to pre-Planck values of cosmological parameters and are close to the parameters found in our main analysis. Since the survey cross-spectra contain less data than the detector set cross-spectra, some shifts are expected and one cannot immediately conclude that this is due to a systematic. However, as shown in Figure 8, the cosmological parameters from uncleaned survey cross-spectra agree well with with those derived from cleaned survey cross-spectra for comparable f_{sky}. For the uncleaned survey cross-spectra we use the same galactic and point-source masks used by Planck. After masking the survey strip, we denote the mask used for the 100 GHz data SA39 and that used for the 143 and 217 GHz data SA24. The figure also shows that parameters derived from cleaned survey cross-spectra show no strong dependence on f_{sky}. This suggests that these shifts are not purely statistical even in the absence of detailed simulations.

We have also analyzed the publicly available halfring maps and compare the results of our analysis based on Planck's foreground model with detector set and season cross-spectra in VI. The halfring cross-spectra contain more data than the survey cross-spectra. However, they contain a small amount of correlated noise that is hard to model. So we do not use them for our main analysis and only use them to check the dependence of cosmological parameters on pixels that were only observed in one of the surveys. As shown in table VI, there is a surprisingly strong sensitivity of cosmological parameters to these pixels. The analysis in which only pixels observed in both surveys are used (Survey $1 \cap 2$) leads to parameters close to those found in our main analysis. As pixels only observed in one of the surveys are added (Survey $1 \cup 2$), the values of the cosmological parameters shift close to those reported by the Planck team. These pixels would be especially problematic if there were a systematic in one of the surveys. Refining further and including pixels only observed in Survey 1 or pixels only observed in Survey 2, we find that the shift entirely derives
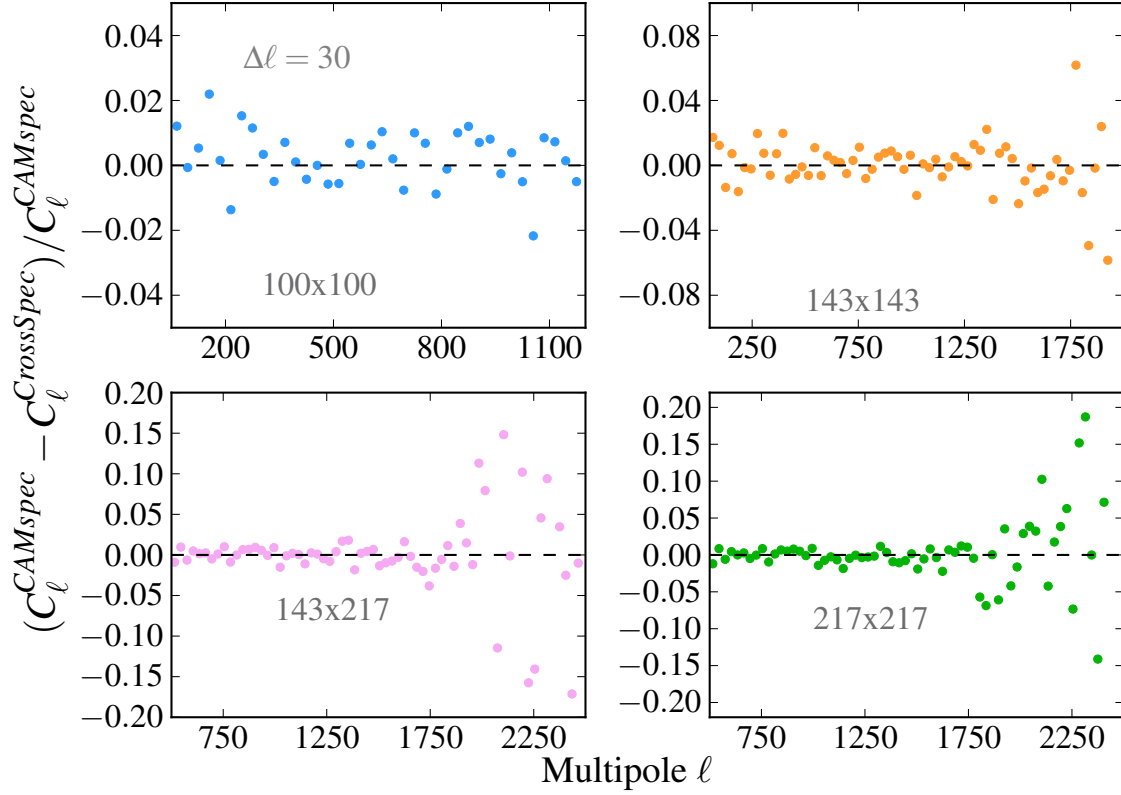
FIG. 12: Season cross and detector set spectra: the Planck CAMspec spectra compared to those computed from the season maps, but using the same masking and galactic foreground modelling procedure as outlined in the Planck likelihood paper. The $\ell \sim 1800$ feature is not present in the cross season spectra even without any additional cleaning procedure applied.

from the pixels only observed in Survey 1. In contrast, including pixels only observed in Survey 2 only has a small effect on cosmological parameters. The shifts are too large to be caused by the amount of data added, suggesting either a systematic in these pixels or that the sky happens to be peculiar in the strip only observed in Survey 1.

VI. CONCLUSION

Because of their exquisite sensitivity, the Planck data are our most sensitive measurement of cosmological parameters and the basic properties of our universe. Because of this sensitivity, it is important that there are independent analyses of the Planck data to complement the work done by the Planck team.

We have performed such an independent analysis and have found that the 217×217 data drives the tension between cosmological parameters determined from the CMB and those determined from astronomical measurements. Re-analyzing the Planck maps and using only the season cross-spectra, we find cosmological parameters more consistent with other measurements. This suggests that the tension is at least in part due to cross-correlations between 217 detectors observing the sky at the same time. Whether this is a statistical fluke or a signature of a residual systematic in the 217 GHz maps is difficult to determine with the current data. However, the upcoming release and analysis of the full five seasons of Planck data should clarify this issue and provide even more detailed insights into the basic properties of our universe.

Acknowledgments

[1] D. N. Spergel, L. Verde, H. V. Peiris, et al., ApJS **148**, 175 (2003), arXiv:astro-ph/0302209.
[2] D. N. Spergel, R. Bean, O. Doré, et al., ApJS **170**, 377 (2007), arXiv:astro-ph/0603449.
[3] J. Dunkley, D. N. Spergel, E. Komatsu, et al., ApJ **701**, 1804 (2009), 0811.4280.
[4] E. Komatsu, K. M. Smith, J. Dunkley, et al., ApJS **192**, 18 (2011), 1001.4538.
[5] G. Hinshaw, D. Larson, E. Komatsu, et al., ArXiv e-prints (2012), 1212.5226.
[6] J. L. Sievers, R. A. Hlozek, M. R. Nolta, et al., ArXiv e-prints (2013), 1301.0824.
[7] K. T. Story, C. L. Reichardt, Z. Hou, et al., ArXiv e-prints (2012), 1210.7231.
[8] P. A. R. Ade *et al.* [Planck Collaboration (I)], Astron. Astrophys. **571**, A1 (2014) [arXiv:1303.5062 [astro-ph.CO]].
[9] P. A. R. Ade *et al.* [Planck Collaboration (XV)], Astron. Astrophys. **571**, A15 (2014) [arXiv:1303.5075 [astro-ph.CO]].
[10] P. A. R. Ade *et al.* [Planck Collaboration (XVI)], Astron. Astrophys. **571**, A16 (2014) [arXiv:1303.5076 [astro-ph.CO]].
[11] E. Calabrese, R. A. Hlozek, N. Battaglia, et al., Phys. Rev. D **87**, 103012 (2013), 1302.1841.
[12] A. G. Riess, L. Macri, S. Casertano, et al., ApJ **730**, 119 (2011), 1103.2976.
[13] W. L. Freedman, B. F. Madore, V. Scowcroft, et al., ApJ **758**, 24 (2012), 1208.3281.
[14] A. Conley, J. Guy, M. Sullivan, et al., ApJS **192**, 1 (2011), 1104.1443.
[15] E. M. Huff, T. Eifler, C. M. Hirata, et al., ArXiv e-prints (2011), 1112.3143.
[16] C. Heymans, E. Grocutt, A. Heavens, et al., MNRAS **432**, 2433 (2013), 1303.1808.
[17] P. A. R. Ade *et al.* [Planck Collaboration (XXI)], Astron. Astrophys. **571**, A21 (2014) [arXiv:1303.5081 [astro-ph.CO]].
[18] T. M. Crawford, K. K. Schaffer, S. Bhattacharya, et al., ArXiv e-prints (2013), 1303.3535.
[19] M. J. Wilson, B. D. Sherwin, J. C. Hill, et al., Phys. Rev. D **86**, 122005 (2012), 1203.6633.
[20] C. L. Reichardt, L. Shaw, O. Zahn, et al., ApJ **755**, 70 (2012), 1111.0932.
[21] P. A. R. Ade *et al.* [Planck Collaboration (XX)], Astron. Astrophys. **571**, A20 (2014) [arXiv:1303.5080 [astro-ph.CO]].
[22] A. Vikhlinin, A. V. Kravtsov, R. A. Burenin, et al., ApJ **692**, 1060 (2009), 0812.2720.
[23] A. Hajian, N. Battaglia, D. N. Spergel, et al., ArXiv e-prints (2013), 1309.3282.
[24] M. Cacciato, F. C. van den Bosch, S. More, et al., MNRAS **430**, 767 (2013), 1207.0503.
[25] P. A. R. Ade *et al.* [Planck Collaboration (VI)], Astron. Astrophys. **571**, A6 (2014) [arXiv:1303.5067 [astro-ph.CO]].
[26] P. A. R. Ade *et al.* [Planck Collaboration (XII)], Astron. Astrophys. **571**, A22 (2014) [arXiv:1303.5082 [astro-ph.CO]].
[27] S. Das, T. Louis, M. R. Nolta, et al., ArXiv e-prints (2013), 1301.1037.
[28] Z. Hou, C. L. Reichardt, K. T. Story, et al., ArXiv e-prints (2012), 1212.6267.
[29] P. A. R. Ade *et al.* [Planck Collaboration (XII)], Astron. Astrophys. **571**, A12 (2014) [arXiv:1303.5072 [astro-ph.CO]].
[30] A. Lewis, A. Challinor, A. Lasenby, Astrophys. J. **538**, 473 (2000), astro-ph/9911177.
[31] A. Lewis, S. Bridle, Phys. Rev. D **66**, 103511 (2002), astro-ph/0205436.
[32] G. Efstathiou, ArXiv e-prints (2013), 1311.3461.
[33] S. H. Suyu, T. Treu, S. Hilbert, et al., ArXiv e-prints (2013), 1306.4732.
[34] K. M. Gorski, T. Hivon, S. Banday, et al., Astrophys. J. **622**, 759 (2005), astro-ph/0409513.